J Solid State Electrochem (2012) 16:1767–1774
DOI 10.1007/s10008-012-1669-8

ORIGINAL PAPER

Nanocrystalline tin compounds/graphene nanocomposite electrodes as anode for lithium-ion battery

Marappan Sathish · Satoshi Mitani · Takaaki Tomai · Atsushi Unemoto · Itaru Honma

Received: 22 August 2011 / Revised: 24 January 2012 / Accepted: 28 January 2012 / Published online: 22 February 2012

Abstract Nanocrystalline tin (Sn) compounds such as SnO_2, SnS_2, SnS, and graphene nanocomposites were prepared using hydrothermal method. The X-ray diffraction (XRD) pattern of the prepared nanocomposite reveals the presence of tetragonal SnO_2, hexagonal SnS_2, and orthorhombic SnS crystalline structure in the SnO_2/graphene nanosheets (GNS), SnS_2/GNS, and SnS/GNS nanocomposites, respectively. Raman spectroscopic studies of the nanocomposites confirm the existence of graphene in the nanocomposites. The transmission electron microscopy (TEM) images of the nanocomposites revealed the formation of homogeneous nanocrystalline SnO_2, SnS_2, and SnS particle. The weight ratio of graphene and Sn compound in the nanocomposite was estimated using thermogravimetric (TG) analysis. The cyclic voltammetry experiment shows the irreversible formation of Li_2O and Li_2S, and reversible lithium-ion (Li-ion) storage in Sn and GNS. The charge–discharge profile of the nanocomposite electrodes indicates the high capacity for the Li-ion storage, and the cycling study indicates the fast capacity fading due to the poor electrical conductivity of the nanocomposite electrodes. Hence, the ratio of Sn compounds (SnO_2) and GNS have been altered. Among the examined SnO_2:GNS nanocomposites ratios (35:65, 50:50, and 80:20), the nanocomposite 50:50wt% shows high Li-ion storage capacity (400 mAh/g after 25 cycles) and good cyclability. Thus, it is necessary to modify GNS and Sn compound composition in the nanocomposite to achieve good cyclability.

Keywords Li-ion battery · Graphene · Energy storage · Tin oxide · Tin sulfide

M. Sathish (✉) · S. Mitani · T. Tomai · A. Unemoto · I. Honma (✉)
Institute of Multidisciplinary Research for Advanced Materials, Tohoku University,
2-1-1, Katahira, Aoba-Ku,
Sendai 980-8577, Japan
e-mail: marappan.sathish@gmail.com
e-mail: i.honma@tagen.tohoku.ac.jp

Introduction

Sn-based nanomaterials have created much attention in materials chemistry owing to their potential application in Li-ion batteries [1]. The present anode material, graphite, has an inherent limitation with a theoretical gravimetric capacity of 372 mAh/g [2]. Sn-based nanomaterials show a large theoretical capacity value due to the formation of Li–Sn alloy, which initiates much effort to explore these materials as anode for Li-ion battery. In recent days, Sn-based materials such as SnO_2, SnS_2, and SnS have been prepared by various techniques with different size and morphology, and explored for Li-ion battery application [3–7]. Among these materials, SnO_2 have been extensively studied. Indeed, the low electrical conductivity and large volume expansion/contraction (during charging and discharging) results poor cyclability. Thus, the practical application of these materials has not been attained so far. To overcome the above issues, attempts have been made to prepare nanostructured materials with diverse morphologies such as nanosheets, nanorods, nanoparticle, and nanoplates etc. [8–10]. Reducing the particle size will increase the surface to volume ratio and that would decrease the volume changes during the Li insertion and extraction. Also, it is proposed that preparation of layered crystalline nanostructured materials similar to the structure of graphite can minimize the volume change during cycling and offer more active cites for the accommodation of Li-ions [11]. SnS_2 has a layered

CdI_2 crystalline like structure composed of Sn atoms sandwiched between two layers of hexagonally disposed close-packed sulfur atoms and the neighboring sulfur layers are connected with week van der Waals forces. This crystallographic feature is suitable for both the intercalation of Li-ions and the compensation of the alloying/dealloying volume change. Thus, the Li-ion can easily access the Sn atoms in the SnS_2 structure, and the resulting volume change could be easily controlled without any structural damage. However, only limited attempts have been made to prepare SnS_2 nanostructured materials for Li-ion storage application owing to their poor electrical conductivity [12–18].

The addition of conducting carbon materials such as acetylene black, graphene, etc. will increase the conductivity of the materials. The recent progress in the graphene nanosheets (GNS) as high surface area and good conductive support for nanocomposite electrode materials opens a new avenue in materials chemistry [19, 20]. The availability of large surface area in the GNS facilitates the homogeneous distribution of nanoparticles on its surface. Consequently, various metal oxides–GNS nanocomposites have been successfully prepared using different synthetic strategies and demonstrated for various applications [21–24]. Particularly, SnO_2/GNS nanocomposite electrodes have been prepared and superior Li-ion storage properties have been reported [25–27]. Interestingly, the Li-ion storage capability of GNS in the nanocomposites offers further advantages to the nanocomposites. In addition, the dispersion of nanoparticle on the GNS hinders the re-stacking of GNS that would also increase the Li-ion storage capacity of GNS. In this present study, SnO_2/GNS, SnS_2/GNS, and SnS/GNS nanocomposite electrode materials were prepared using hydrothermal method. The prepared nanocomposite electrode materials were characterized using X-ray diffraction (XRD), TEM, thermogravimetric (TG), cyclic voltammetry, and galvanostatic charge–discharge measurements. The electrochemical response of the prepared nanocomposite electrodes was studied using cyclic voltammetry and galvanostatic charge–discharge measurements.

Experimental section

Graphene oxide synthesis

Graphene oxide dispersion (15 mg/mL) was prepared by modified Hummers and Offeman's method reported elsewhere [28, 29]. In a typical preparation, 0.5 g of graphite powder (Sigma Aldrich, 5–20 μm), 0.5 g of $NaNO_3$, and 23 mL of H_2SO_4 were stirred together in an ice water bath. Then, 3 g of $KMnO_4$ was slowly added. Once mixed, the solution was transferred to a 35±5 °C water bath and stirred for about 1 h, forming a thick paste. Forty milliliters of water was added to the above paste and the resulting solution was stirred for 30 min while the temperature was raised to 90±5 °C. Finally, 100 mL of water containing 3 mL of H_2O_2 was added, the color of the solution turns from dark brown to yellow. The warm solution was then filtered and washed with 200 mL of water. The filter cake was then dispersed in water by mechanical agitation. Low-speed centrifugation was done at 1,000 rpm for 5 min and the visible particles were removed completely from the precipitates. The supernatant then underwent two more high-speed centrifugation steps at 8,000 rpm for 15 min to remove small GO pieces and water-soluble by-products. The final sediment was re-dispersed in water with mechanical agitation and mild sonication, giving a solution of exfoliated GO.

SnO_2/GNS synthesis

In a typical preparation, 0.95 g of $SnCl_4{\cdot}5H_2O$ (Wako, Japan) in 15 ml water was added to graphene oxide solution (15 mL, ~15 mg/mL) and the solution was stirred for 30 min vigorously and ultrasonicated for 30 min. Then, 0.25 g of NH_4OH (Wako, Japan) solution was added drop wise and the resulting mixture was put in to Teflon lined stainless steel autoclave and heat treated at 180 °C for 15 h. The resulting nanocomposite powder was washed with ethanol and water, and dried at 60 °C overnight. SnO_2 loading on GNS have been varied by altering the concentration of $SnCl_4{\cdot}5H_2O$ and keeping the GO solution as constant.

SnS_2/GNS synthesis

In a typical preparation, 0.85 g of $SnCl_4{\cdot}5H_2O$ (Wako, Japan) and 0.75 g of thiourea (Sigma Aldrich) mixture in 15 mL water was added to graphene oxide solution (15 mL, ~15 mg/mL) and the solution was stirred for 30 min vigorously and ultrasonicated for 30 min. The resulting solution mixture was put into Teflon lined stainless steel autoclave and heat treated at 180 °C for 15 h. The resulting nanocomposite powder was washed with ethanol and water, and dried at 60 °C overnight. The as-prepared nanocomposite was further reduced using hydrazine solution at 90 °C for 3 h.

SnS/GNS synthesis

The as-prepared nanocomposite obtained in the previous step (SnS_2/GNS) was reduced in H_2-Ar (10:90) mixture at 400 °C for 3 h.

Material characterization

XRD patterns were collected on a RIGAKU (RINT2000 Tokyo, Japan) diffractometer using Ni-filtered Cu-K_α radiation (λ=1.5418 Å). TG experiments (SII, TG/DTA 6300)

were conducted in a temperature range of 25–1000 °C and in an air atmosphere using ~5–10 mg of the sample at the heating rate of 10 °C/min. Scanning and high-resolution transmission electron micrographs (STEM and HR-TEM) were recorded with a JEOL JEM-2100F microscope, working at an accelerating voltage of 200 kV. The structure of the obtained nanocomposites was characterized using a micro-Raman system (HORIBA Scientific, Japan) equipped with a semiconducting laser with a wavelength of 532 nm.

Electrochemical evaluation

The working electrodes were fabricated by mixing 95 wt% active material and 5 wt% polytetrafluoroethylene (used as a binder, PTFE, Sigma Aldrich) and pressed on Ni mesh. For bulk SnO_2 nanoparticles, 85 wt% sample, 10 wt% acetylene black, and 5 wt% PTFE was added to make the electrode paste and pressed on Ni mesh. The electrodes were dried in a vacuum oven at 120 °C overnight before transferring into an Argon-filled glove box. Conventional three electrode cells were fabricated using lithium metal as the counter electrode and reference electrode, and $LiClO_4$ (1 M) in ethylene carbonate/diethyl carbonate (EC/DEC, 1:1 vol%) as the electrolyte. The electrochemical performances of the prepared electrodes were characterized by cyclic voltammetry (Solartron 1260, USA) and galvanostatic charge–discharge (HOKUTO DENKO, Japan) test between 0.001 V and 1.2 V vs Li/Li+.

Results and discussion

In Fig. 1, the XRD pattern of SnO_2/GNS, SnS_2/GNS, and SnS/GNS nanocomposites were compared. In all the nanocomposites, diffraction line corresponding to GNS could not be seen, this clearly indicates uniform dispersion of GNS in the nanocomposites. The SnO_2/GNS nanocomposite (Fig. 1a) shows clear diffraction lines corresponding to tetragonal crystalline structure of SnO_2 with a calculated lattice parameters of a=4.726 Å and c=3.185 Å [JCPDS 77–0452]. Similarly, the SnS_2/GNS and SnS/GNS nanocomposites show hexagonal SnS_2 (JCPDS: 23–677) and orthorhombic (JCPDS: 39–354) crystalline structure, respectively. And, the calculated lattice parameters a=3.635 Å and c=5.884 Å for the former case and a=4.300 Å, b=11.164 Å and c=3.967 Å for the latter case are in good agreement with JCPDS data (JCPDS: 39–354). This clearly indicates that the reduction of SnS_2 at high temperature (400 °C) in H_2/Ar atmosphere results the formation SnS. In addition, the impurities (shown as * in Fig. 1c) corresponding to 001 and 101 plane of SnS_2 structure indicates the existence of residual SnS_2in the SnS/GNS nanocomposite.

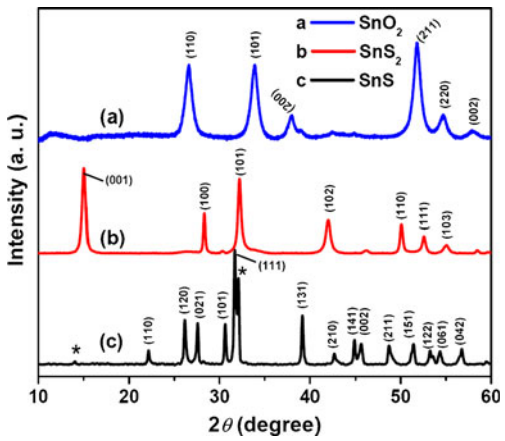

Fig. 1 XRD pattern of (**a**) SnO_2/GNS, (**b**) SnS_2/GNS, and (**c**) SnS/GNS nanocomposite electrodes

The amount of Sn compound (SnO_2, SnS_2, SnS) dispersions on the GNS in the nanocomposites were estimated using TG profile between 25 and 900 °C in air. In Fig. 2A, the TG profile of nanocomposites (a) SnO_2/GNS, (b) SnS/GNS, and (c) SnS_2/GNS were compared. SnO_2/GNS nanocomposite shows a decomposition profile with 18% weight loss from 400 °C to 650 °C regions owing to the decomposition of GNS. Whereas, the SnS_2/GNS nanocomposite shows two-stage weight loss (34 wt%) from 230 to 450 °C and from 450 to 650 °C. It is well known that the SnS_2 will undergo oxidation at high temperature that will result the formation of SnO_2. Thus, a partial weight loss (20 wt%) was observed between 230 and 450 °C. The second weight loss (14 wt%, between 450 and 650 °C) could be ascribed to the decomposition of GNS. SnS/GNS nanocomposite shows a weight loss similar to the SnO_2 profile due to the similar molecular weight of SnS and SnO_2. The oxidation at high temperature does not make significant change in the TG profile from 230 to 450 °C. However, a very small weight loss (~5 wt%) was observed in that range due to the SnS_2 present as impurity in the SnS/GNS nanocomposite. In addition, a 17% weight loss was observed at high temperature (450–650 °C) due to the decomposition of GNS. Further, SnO_2 loading on GNS has been varied by altering the SnO_2 precursor weights during the preparation. Three different nanocomposites were prepared with different SnO_2 loading on GNS and the exact amount of SnO_2 loading in the final nanocomposites was estimated using TGA. Figure 2B shows the decomposition profile of SnO_2/GNS nanocomposites and the calculated weight ratio of SnO_2 and GNS in the nanocomposites are (a) 80:20, (b) 50:50 and (c) 35:65 wt%.

Further insights of the structural and electronic properties of GNS in the nanocomposite are obtained from Raman spectroscopy characterization. Figure 3 shows Raman spectra of all the nanocomposites and pure GNS prepared under the same experimental condition, and it clearly demonstrate the characteristic D and G bands around 1,333 and 1,570 cm^{-1},

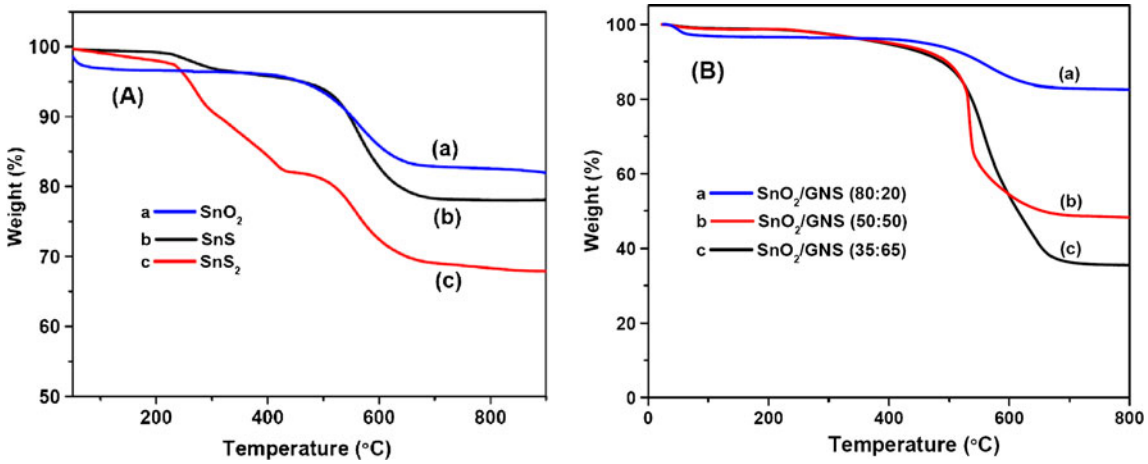

Fig. 2 **A** TG profiles of (*a*) SnO_2/GNS, (*b*) SnS/GNS, and (*c*) SnS_2/GNS nanocomposite. **B** TG profiles of SnO_2/GNS nanocomposites (*a*) 80: 20, (*b*) 50:50 and (*c*) 35: 65 wt%

respectively. On the other hand, the characteristic D and G bands of carbon materials are observed at around 1,350 and 1,585 cm^{-1}, respectively [30, 31]. The D band is associated with disordered samples or graphene edges, while the G band is the result of the first-order scattering of the E_{2g} mode of sp^2 carbon domains. Both bands can be influenced by structural changes. There are many factors, which can affect the position of the D and G band, such as doping, layer numbers, defects, strains, substrate, etc. [32–34]. Thus, it is surmised that the observed down shift in both D and G bands are due to the highly disordered nature of graphene support. The high intensity of D band than the G band for the nanocomposites and pure GNS supports to our speculation. The presence of highly disordered GNS would be a better support for the SnO_2, SnS_2, and SnS nanoparticles. There may be a chemical interaction between the nanoparticles and GNS. More additional experiments are necessary to reveal the above chemical interactions.

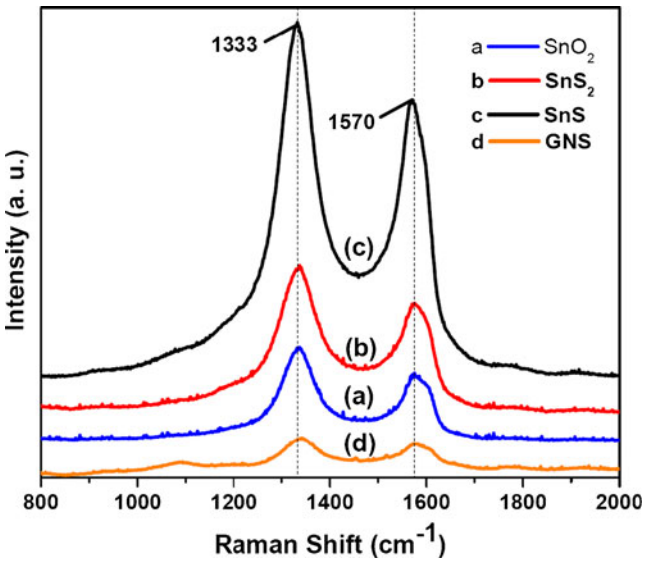

Fig. 3 Raman Spectra of (**a**) SnO_2/GNS, (**b**) SnS_2/GNS, (**c**) SnS/GNS nanocomposites, and (**d**) GNS prepared using the same experimental condition

The morphology and particle size of the prepared nanocomposites have been analyzed using TEM microscopy and shown in Fig. 4. The TEM images of nanocomposites observed at different magnifications shows a clear version of the nanoparticle distribution on GNS support. The TEM images of SnO_2/GNS (Fig. 4a, b) show the presence of agglomerated SnO_2 nanoparticle on GNS surface. This clearly indicates that the amount of SnO_2 in the nanocomposite is too high or GNS surface was not utilized effectively. The observed 18:82 wt% ratio of GNS and SnO_2 in the SnO_2/GNS by TG experiments indicates that the amount of SnO_2 in the composite is high and it should be reduced for better distribution. The TEM images of SnS_2/GNS (Fig. 4c, d) show a plate like SnS_2 nanodisks and GNS composite; the observed morphology of the SnS_2 is similar to the recently reported SnS_2 nanoplates by Zhai et al. [12] and Seo et al. [14]. Interestingly, when this SnS_2/GNS nanocomposite reduced in H_2 atmosphere at high temperature, SnS/GNS nanocomposite was formed that shows nanoparticle of SnS with ~10 nm size on GNS surface. Indeed, the nanodisk morphology was transformed to uniform SnS nanoparticle (Fig. 4e, f). This clearly indicates that the high temperature treatment in H_2 atmosphere reduce the SnS_2 to SnS and induces the morphological transformation from nanodisk to nanoparticles. The formation of uniform size SnS nanoparticle on GNS surface by the decomposion of SnS_2 nanodisk supports our earlier speculation of chemical interaction between the Sn compounds and GNS.

To explore the potential applications of the above synthesized nanocomposite materials, the samples were fabricated into electrodes and characterized with galvanostatic charge/discharge measurements and cyclic voltammetry (CV) analysis. Figure 5a–c shows the charge–discharge profile (1st, 2nd, 5th, and 25th cycles) of the nanocomposite

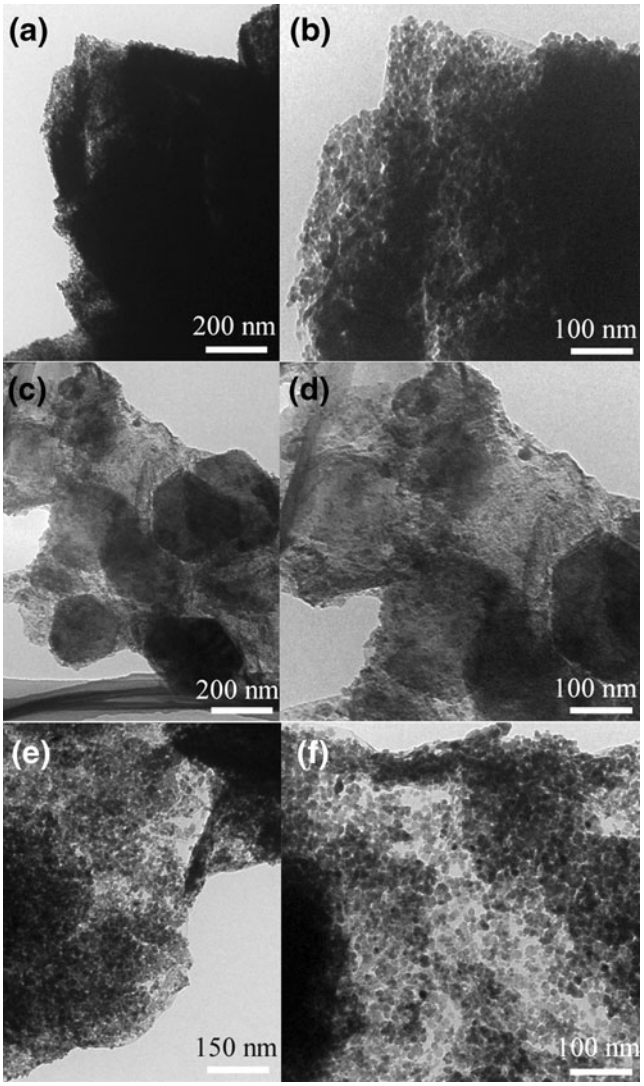

Fig. 4 Representative TEM images of **a** and **b** SnO_2/GNS, **c** and **d** SnS_2/GNS and **e** and **f** SnS/GNS nanocomposites at different magnifications

electrodes at 0.1 C current density. All three samples show a high irreversible capacity during the first cycle owing to the formation of Li_2S and Li-Sn alloy as shown in Eq. 1–5. It could be clearly seen from the charge–discharge profile (Fig. 5a) that the reversible capacity of SnO_2/GNS nanocomposite observed for the 2nd cycle (~500 mAh/g) was rapidly decreasing with cycles and reached 200 mAh/g after 25 cycles. Similarly, SnS_2/GNS and SnS/GNS nanocomposites show 485 mAh/g and 390 mAh/g in the 2nd discharge and the capacity decrease to 200 mAh/g and 210 mAh/g in the 25th cycle, respectively. This is ascribed to the poor electrical conductivity of the nanocomposites that contains insufficient GNS or excess Sn compounds. It is worthy to mention here that no other conductive carbon (acetylene black) was added during the electrode fabrication. Thus it is believed that the GNS used as support for the Sn compounds is not sufficient enough for high capacity retention. However, an attempt has been made to evaluate the performance of the prepared nanocomposite electrodes by making a comparison with their theoretical capacity. The theoretical capacity of the nanocomposite was calculated based on their composition (obtained from TG analysis) as shown by the following equation.

$$C_{Theoretical} = C_{SnO2} \times \%_{mass\ of\ SnO2} + C_{graphite} \times \%_{mass\ of\ graphite} = (782 \times 0.82 + 372 \times 0.18) = 708\ mAh/g$$

Similarly, 606 mAh/g and 712 mAh/g were calculated for the SnS_2/GNS and SnS/GNS nanocomposites by taking the theoretical capacity of SnS_2 and SnS as 645 mAh/g and 782 mAh/g, respectively. Figure 5d shows the capacity comparison of nanocomposites with number of cycles. The plot indicates that the order of Li-ion storage capacity of the nanocomposite electrodes is SnS/GNS > SnO_2/GNS > SnS_2/GNS. However, by comparing their theoretical capacity, the order becomes SnS_2/GNS (80%) > SnO_2/GNS (70%) > SnS/GNS (55%).

Attempts have been made to vary the amount of SnO_2 loading on the GNS, and their effect on the Li-ion charge–discharge behavior of the nanocomposties has been studied. Thus, three different SnO_2/GNS nanocomposites with a weight ratio (%) of 80:20, 50:50, and 35:65 were prepared by altering the SnO_2 precursors during the preparation of the nanocomposite. The final composition (weight ratio in%) of the prepared SnO_2/GNS was estimated using TGA (Fig. 2b). Bulk SnO_2 was also prepared using the same experimental condition (without GO solution) for comparison purpose. Figure 6 shows the Li-ion storage capacity of the above nanocomposites for 25 cycles. It could be very clearly seen that SnO_2/GNS nanocomposites show better Li-ion storage capacity compared to bulk SnO_2 nanoparticles. In addition, the cyclability of the nanocomposites is also very stable compared to bulk SnO_2 nanoparticles. SnO_2/GNS nanocomposite with a weight ratio (%) of 35:65 shows Li-ion storage capacity of 300 mAh/g after 25 cycles (Fig. 6a). When increasing the SnO_2 weight in the nanocomposite (50 wt %), the capacity also increase to 400 mAh/g after 25 cycles (Fig. 6b). However, when the amount of SnO_2 in the SnO_2/GNS nanocomposite is high (80 wt%), capacity fading behavior could be seen after 15 cycles and the Li-ion storage capacity decreases to 200 mAh/g after 25 cycles. The GNS with 50 and 35 wt% SnO_2 show excellent cyclability, owing to the small volume expansion–contraction and availability of large dead volume in the GNS inter-layers to accommodate the above small volume expansion–contraction with sufficient electrical and electronic contacts.

To understand the Li-ion insertion and extraction process in the nanocomposite electrodes during discharge and charge process, cyclic voltammogram was measured between 0.001 V and 3 V vs Li/Li^+ at the scan rate of 0.1 mV/s.

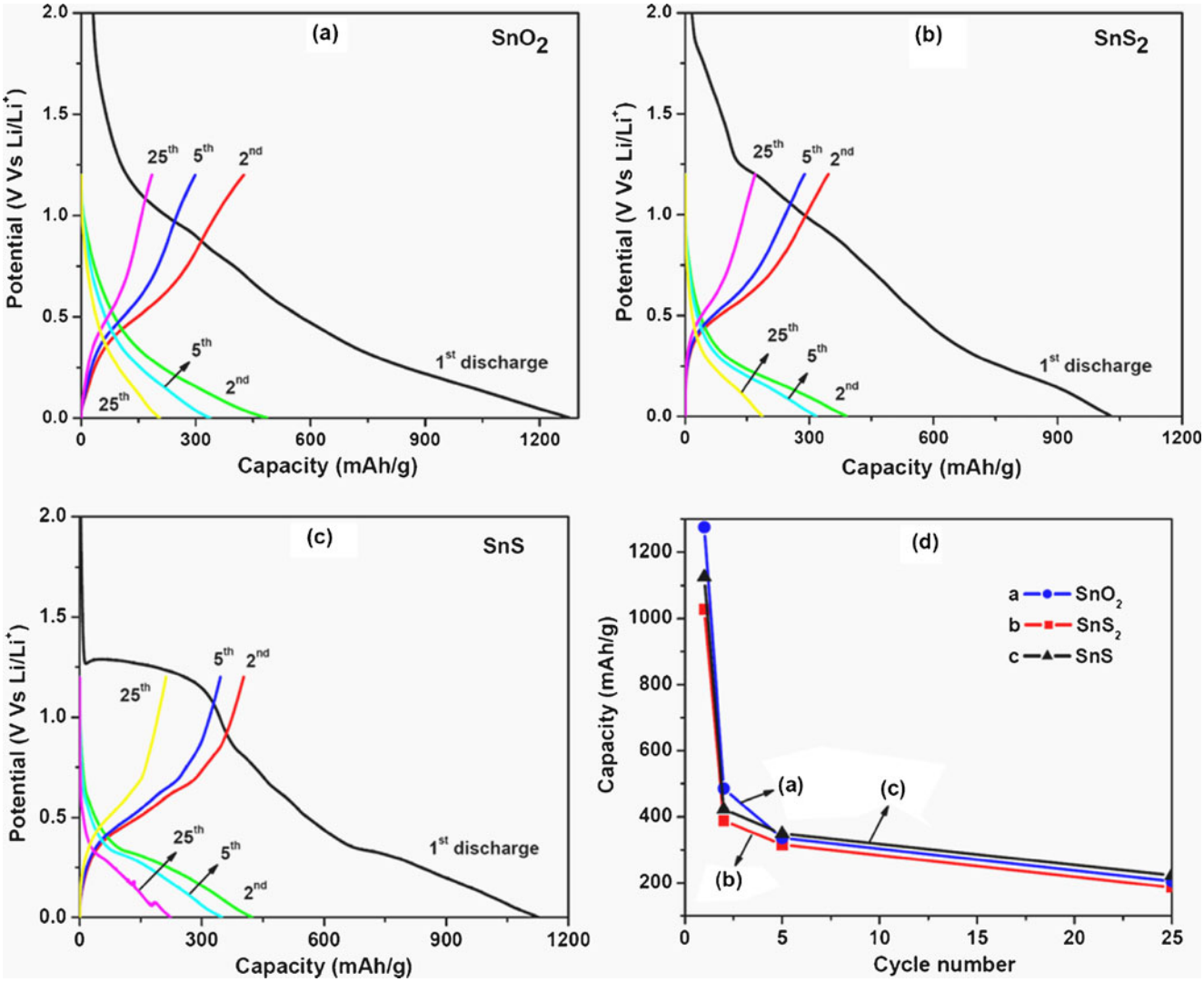

Fig. 5 Galvanostatic charge–discharge profiles of **a** SnO_2/GNS, **b** SnS_2/GNS, and **c** SnS/GNS nanocomposite electrodes at 0.1C current density. **d** Capacity comparison profile of all three electrodes from 1 to 25 cycles

Figure 7A–C shows the first two cycles of cyclic voltammetery profile of nanocomposite electrodes and pure GNS (prepared using the same experimental condition). The peak observed below 0.5 V in all the three electrodes indicates reversible formation of Li–Sn alloy and Li intercalation in GNS (Eq. 1 and 5). The SnO_2/GNS did not show characteristic peaks corresponding to the formation of Li_2O as shown in Eq. 2. Whereas, SnS_2/GNS shows three peaks at 0.8, 1.75, and 2.35 V which are attributed to the decomposition of SnS_2 and the formation of Li_2S as shown in Eq. 3 that may occur in several steps as suggested by the Kim et. al. [15]. Also, SnS/GNS shows one sharp peak at 0.8 V and two humps at 1.35 V and 1.65 V owing to the decomposition of SnS and formation of Li_2S and Sn (Eq. 4). In both SnS_2/GNS and SnS/GNS, the above observed characteristic peaks diminish significantly during the 2nd cycle, confirming the irreversible formation of Li_2S. In Fig. 7D, the cyclic voltammetry profiles of GNS and RGO (prepared directly reducing GO with hydrazine, no autoclave condition) were compared to understand the GNS structural changes during autoclave preparation. It could be clearly seen from Fig. 7D that there is no significant difference in the CV profiles of GNS and RGO nanosheets. Both pure GNS and RGO nanosheets show a small hump at 0.64 V and a peak below 0.2 V, owing to Li-ion insertion in graphene sheets. This clearly indicates that the autoclave condition does not affect the graphene structure significantly.

$$C + xLi + xe^- \rightleftarrows LixC \quad (1)$$

$$SnO_2 + 4Li^+ + 4e^- \rightarrow Sn + 2Li_2O \quad (2)$$

$$SnS_2 + 4Li^+ + 4e^- \rightarrow Sn + 2Li_2S \quad (3)$$

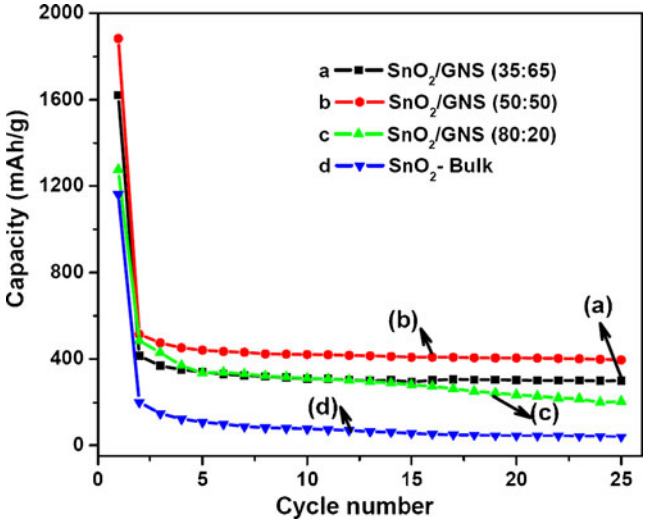

Fig. 6 Capacity vs cycle number profile of SnO_2/GNS nanocomposites with different SnO_2:GNS weight ratio (**a**) 35: 65 (**b**) 50:50 (**c**) 80: 20 and (**d**) Bulk SnO_2 nanoparticles

$$SnS + 2Li^+ + 2e^- \rightarrow Sn + Li_2S \quad (4)$$

$$Sn + xLi + xe^- \rightleftarrows LixSn (0 \leq x \geq 4.4) \quad (5)$$

Conclusions

Nanocrystalline Sn compounds (SnO_2, SnS_2, SnS) and GNS nanocomposites were successfully prepared using hydrothermal method. The presence of tetragonal SnO_2, hexagonal SnS_2, and orthorhombic SnS crystalline structure in the SnO_2/GNS, SnS_2/GNS, and SnS/GNS nanocomposites was revealed by XRD pattern, respectively. TEM studies on the nanocomposites confirm the presence of SnO_2 and SnS nanoparticles, and SnS_2 nanoplates on the GNS surface. In addition, their composition was estimated using TG profiles.

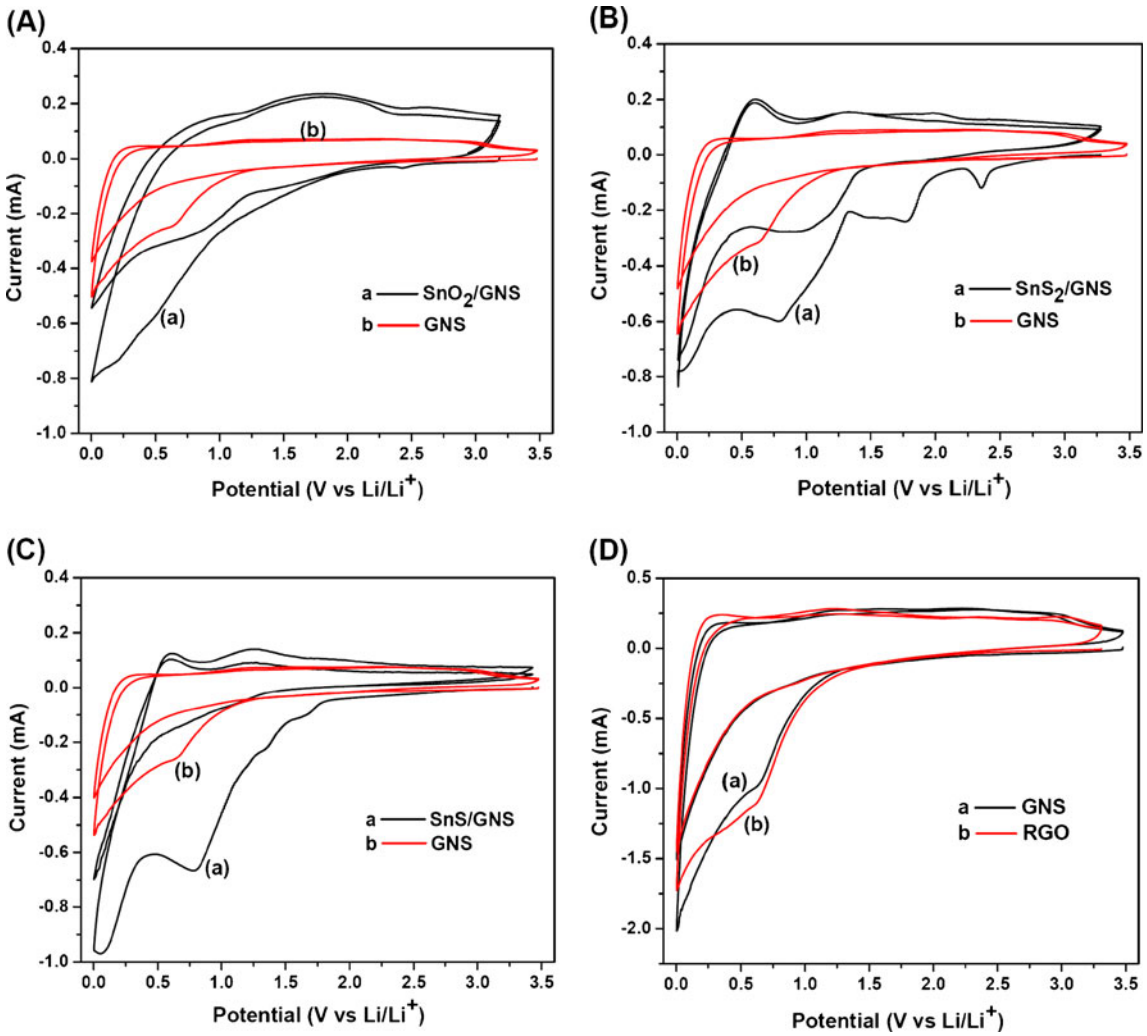

Fig. 7 Cyclic voltammetry profiles of **A** SnO_2/GNS, **B** SnS_2/GNS, **C** SnS/GNS nanocomposite electrodes in comparison with pure GNS electrode at 0.1 mV/s scan rate. **D** GNS and RGO (prepared directly by reducing GO)

The Raman spectroscopy confirms the existence of GNS, and the observed D and G band shift indicates the nature of the GNS. The charge–discharge studies on the nanocomposite indicate the high capacity of the nanocomposites for Li-ion storage at the initial cycles. The fast capacity fading in the subsequent cycles reveals the poor conductivity of the nanocomposites. The ratio of Sn compounds (SnO_2) and GNS have been altered; among the examined SnO_2:GNS nanocomposites ratios (35:65, 50:50, and 80:20), the nanocomposite with 50:50 wt% shows high Li-ion storage capacity (400 mAh/g after 25 cycles) and good cyclability. Thus, GNS amount in the nanocomposite should be optimum to achieve homogeneous dispersion of Sn compounds on the GNS surface and better cyclability. Studies on the cyclic voltammetry confirm the irreversible formation of Li_2S and Li_2O and reversible Li-ion storage in Sn and GNS.

Acknowledgment The author M. Sathish thanks Japan Society for the Promotion of Science (JSPS) for a research fellowship.

References

1. Derrien G, Hassoun J, Panero S, Scrosati B (2007) Adv Mater 19:2336–2340
2. Winter M, Besenhard JO, Spahr ME, Novak P (1998) Adv Mater 10:725–763
3. Idota Y, Kubota T, Matsufuji A, Maekawa Y, Miyasaka T (1997) Science 276:1395–1397
4. Dai ZR, Pan ZW, Wang ZL (2003) Adv Funct Mater 13:9–24
5. Cheng B, Russell JM, Shi WS, Zhang L, Samulski ET (2004) J Am Chem Soc 126:5972–5973
6. Larcher D, Beattie S, Morcrette M, Edstroem K, Jumas JC, Tarascon JM (2007) J Mater Chem 17:3759–3772
7. Yang J, Takeda Y, Imanishi N, Yamamoto O (1999) J Electrochem Soc 146:4009–4013
8. Li Y, Lv X, Lu J, Li J (2010) J Phys Chem C114:21770–21774
9. Kim JG, Nam SH, Lee SH, Choi SM, Kim WB (2011) ACS Appl Mater Interfaces 3:828–835
10. Xu J, Jia C, Cao B, Zhang WF (2007) Electrochim Acta 52:8044–8047
11. Rowsell JLC, Pralong V, Nazar LF (2001) J Am Chem Soc 123:8598–8599
12. Zhai C, Du N, Yang H, Yamg D (2011) Chem Commun 47:1270–1272
13. Liu S, Yin X, Chen L, Li Q, Wang T (2010) Solid State Sciences 12:712–718
14. Seo JW, Jang JT, Park SW, Kim C, Park B (2008) Cheon J. Adv Mater 20:4269–4273
15. Kim TJ, Kim C, Son D, Choi M, Park B (2007) J Power Sources 167:529–535
16. Mukaibo H, Yoshizawa A, Momma T, Osaka T (2003) J Power Sources 119–121:60–63
17. Brousse T, Lee SM, Pasquereau L, Defives D, Schleich DM (1998) Solid State Ionics 113–115:51–56
18. Momma T, Shiraishi N, Yoshizawa A, Osaka T, Gedanken A, Zhu J, Sominski L (2001) J Power Source 97-98:198–200
19. Geim AK (2009) Science 324:1530–1534
20. Geim AK, Novoselov KS (2007) Nat Mater 6:183–191
21. Zhou G, Wang DW, Li F, Zhang L, Li N, Wu ZS, Wen L, Lu GQ, Cheng HM (2010) Chem Mater 22:5306–5313
22. Kim H, Seo DH, Kim SW, Kim J, Kang K (2011) Carbon 49:326–332
23. Wu ZS, Ren W, Wen L, Gao L, Zhao J, Chen Z, Zhou G, Li F, Cheng HM (2010) ACS Nano 4:3187–3194
24. Su J, Cao M, Ren L, Hu C (2011) J Phys Chem C 115:14469–14477
25. Paek SM, Yoo EJ, Honma I (2009) Nano Lett 9:72–75
26. Kim H, Kim SW, Park YU, Gwon H, Seo DH, Kim Y, Kang K (2010) Nano Res 3:813–821
27. Huang X, Zhou X, Zhou L, Qian K, Wang Y, Liu Z, Yu C (2011) ChemPhyChem 12:278–281
28. Hummers WS, Offeman RE (1958) J Am Chem Soc 80:1339
29. Cote LJ, Kim F, Huang J (2009) J Am Chem Soc 131:1043–1049
30. Malard LM, Pimenta MA, Dresselhaus G, Dresselhaus MS (2009) Phys Rep 473:51–87
31. Ferrari AC, Meyer JC, Scardaci V, Casiraghi C, Lazzeri M, Mauri F, Piscanec S, Jiang D, Novoselov KS, Roth S, Geim AK (2006) Phys Rev Lett 97:187401
32. Pisana S, Lazzeri M, Casiraghi C, Novoselov KS, Geim AK, Ferrari AC, Mauri F (2007) Nat Mater 6:198–201
33. Das B, Voggu R, Rout CS, Rao CNR (2008) Chem Commun:5155–5157
34. Das A, Chakraborty B, Sood AK (2008) Bull Mater Sci 31:579–584